Electronic Enhancement of the Exciton Coherence Time in Charged Quantum Dots

G. Moody, C. McDonald, A. Feldman, T. Harvey, R. P. Mirin, and K. L. Silverman[*]

National Institute of Standards and Technology, Boulder, Colorado 80305, USA

Minimizing decoherence due to coupling of a quantum system to its fluctuating environment is at the forefront of quantum information and photonics research. Nature sets the ultimate limit, however, given by the strength of the system's coupling to the electromagnetic field. Here, we establish the ability to electronically control this coupling and enhance the optical coherence time of the charged exciton transition in quantum dots embedded in a photonic waveguide. By manipulating the electronic wave functions through an applied lateral electric field, we increase the coherence time from ∼1.4 to ∼2.7 ns. Numerical calculations reveal that longer coherence arises from the separation of charge carriers by up to ∼6 nm, which leads to a 30% weaker transition dipole moment. The ability to electronically control the coherence time opens new avenues for quantum communication and novel coupling schemes between distant qubits.

In the solid state, three-dimensional quantum confinement of charge carriers in a semiconductor quantum dot (QD) decouples them from their surroundings, resulting in robust optical coherence of the exciton (Coulomb-bound electron-hole pairs) and trion (excitons bound to an additional electron or hole) transitions [1]. The optical coherence time (T_2) is a fundamental property of light-matter interaction, reflecting the time scale during which the ground and excited state excitonic wave functions evolve with a fixed phase relationship [Fig. 1(a)]. From a quantum information perspective, the excitonic coherence time in QDs is a key parameter for quantum phenomena including the duration of Rabi oscillations [2], fidelity of spin-photon entanglement [3], cavity-emitter coupling [4], and single photon purity [5,6].

In the absence of extrinsic decoherence mechanisms, such as exciton-exciton and exciton-phonon scattering, the coherence time is limited by coupling of the excitonic transition to the electromagnetic field. At cryogenic temperatures and low carrier densities, a one-nanosecond T_2 time has been measured corresponding to a sub-μeV homogeneous linewidth $\gamma(\equiv \hbar/T_2)$, which is limited primarily by the spontaneous emission rate $\Gamma(\equiv \hbar/T_1)$, i.e., $T_2 \approx 2T_1$ [see Fig. 1(a)] [7–9]. In this regime, fast and deterministic control of T_2 would be an enabling technology for future QD photonic devices. Simply increasing T_2 would extend the time available for coherent rotations of electronic states about the Bloch sphere. With careful control, one can optimize the trade off between fast rotation times to suit the properties of the source and longevity of the coherence for robust operations. The excitonic coherence time also sets the extent of the single-photon wave packet, which can be leveraged to improve the purity and indistinguishability of photons generated from unique QDs for quantum computing applications [10]. With control of the coherence time faster than $1/T_2$, more advanced operations

such as dynamic tunability of the Rabi frequency and coherent storage of QD qubits can be envisioned.

Despite the above-mentioned utility, control of excitonic coherence in QDs has not been intensely explored. This is especially true when it comes to increasing the coherence time. A large body of work is devoted to manipulating the radiative lifetime of excitonic transitions by embedding QDs in nanostructures with a modified vacuum density of optical states. Large enhancements of the emission rate can be achieved via the Purcell effect, and a reduction of T_1 results in a decrease in T_2 [11–13]. The radiative lifetime can also be increased in these structures, but this has no effect on the coherence time as it is already limited by extrinsic decoherence processes in these cases (so-called "pure dephasing").

Alternatively, one can control the spontaneous emission rate by manipulating the electronic wave functions within the QD using an electric field [14–16]. In the majority of previous studies, carrier tunneling out of the QDs decreased the lifetime; however, the introduction of a high-energy barrier to suppress tunneling led to a factor of 2 increase in the lifetime for vertically [17] and laterally [18] applied electric fields. Despite these advancements in spontaneous emission control, lifetime measurements do not provide any details of the coherent properties of the system. In many experiments, it was extremely likely T_2 was limited by nonradiative recombination and pure dephasing due to background charges and nonresonant excitation of carriers. Moreover, it is not clear whether separation of the electronic wave functions ultimately decreases T_2 due to enhanced interactions with polar optical phonons [19]. Indeed, an increase in the homogeneous linewidth (decrease in T_2) with applied electric field was observed even though the oscillator strength was reduced due to charge separation within the QD [20,21].
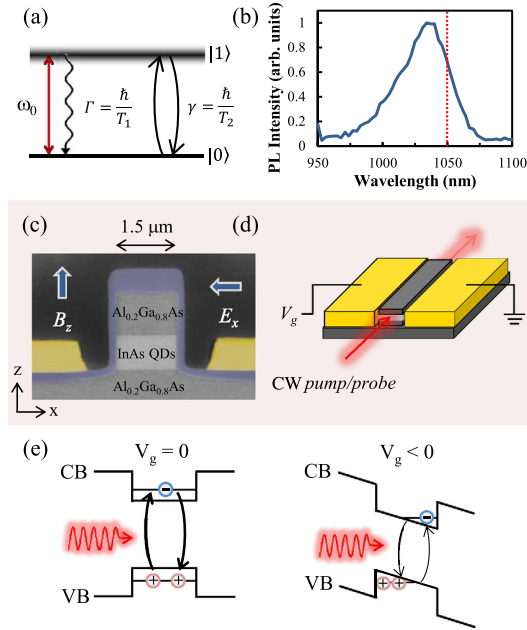
FIG. 1.   (a) The quantum dynamics of a two-level system with resonance frequency ω_0 are governed by spontaneous emission with rate Γ (radiative lifetime T_1) and decoherence with rate γ (coherence time T_2), which defines the homogeneous linewidth. (b) Photoluminescence spectrum taken at 4.2 K showing the inhomogeneously broadened trion transition. The laser wavelength for the nonlinear spectroscopy experiments is indicated by the dashed line. (c) False color scanning electron microscope image of the device and direction of the applied electric (E_X) and magnetic (B_Z) fields. (d) Continuous wave (cw) pump and probe lasers are collinearly coupled into the waveguide for the spectral hole burning measurements. (e) Application of a lateral (x direction) electric field separates the electron and hole wave functions in the QD, which increases the radiative lifetime and coherence time.

In this Letter, we demonstrate a new approach for electronically controlling and enhancing excitonic coherence in QDs. We examine a single layer of charged InAs/GaAs QDs emitting near 1045 nm [see Fig. 1(b) and Supplemental Material [22]]. A photonic ridge waveguide structure is lithographically defined to confine optical modes to the QD region, illustrated by the false color scanning electron microscope image in Fig. 1(c). Gold electrodes are patterned on both sides of the waveguide. Applying a quasistatic voltage bias across the electrodes generates an in-plane electric field up to 15 kV cm^{-1} at the QD region. The applied field depicted in Fig. 1(e) tilts the conduction (CB) and valence (VB) bands in the plane of the device along the x direction. Upon optical excitation of the trion transition, lateral displacement of the electron and holes reduces the radiative efficiency and increases the radiative lifetime. Using high-resolution nonlinear optical spectroscopy, we demonstrate that coherence is maintained during this process and the homogeneous linewidth (coherence time) decreases (increases) by more than a factor of 2.

Since our QDs exhibit a Fourier-limited emission profile under these experimental conditions, we have full control of the coherence time through its fixed relationship to the radiative lifetime.

This device design offers several advantages for electronic coherence control compared to previous studies. First, confinement of the optical modes to the QD region enhances the light-matter interaction. Second, the base diameter of our QDs is much larger than the height. Compared to diode devices generating longitudinal fields along the sample growth direction, a lateral field can generate much larger separation between charges before becoming strong enough to induce significant tunneling out of the QD that destroys coherence. The device also has extremely low capacitance ($\sim$100 fF), offering the possibility of gigahertz frequency control of the coherence time.

The trion coherence time is obtained by measuring the homogeneous linewidth using spectral hole-burning spectroscopy [see Fig. 1(d) and Supplemental Material [22]]. Briefly, continuous-wave pump and probe lasers are coupled into the waveguide, held at 4.2 K in a transmission confocal microscopy setup. The pump laser wavelength is fixed at 1050 nm and partially saturates the absorption of the trion transition in $\approx$10 QDs, burning a spectral "hole" in the inhomogeneous distribution. A probe laser is spectrally tuned through the pump to map out the line shape of the "hole," providing a measure of the homogeneous linewidth. This technique allows for shot-noise limited detection of pump-induced modulation of the probe absorption. Moreover, spectral diffusion processes that typically broaden the excitonic transition linewidth to tens of microelectronvolts in single dot photoluminescence experiments are absent from our ensemble measurements because the characteristic diffusion time constant is much longer than the excitonic transition lifetime T_1 [23]. The sample preparation and geometry enable our electronic control of the trion transition coherence time.

First, we present measurements with zero applied field. Line shapes are shown in Fig. 2(a) for increasing pump power up to 1 nW. The half width at half maximum (HWHM) of the Lorentzian function (solid lines) provides a measure of the homogeneous linewidth and is inversely proportional to the coherence time [24]. Fits using a Voigt line shape are nearly identical to the Lorentzian line shapes with the Gaussian component contributing less than 5%, which supports our assertion that the measurements are free from spectral diffusion. The single Lorentzian line shape also implies that spectral-hole burning and coherent population oscillation contributions to the nonlinear signal spectrally overlap with similar linewidths, indicating that the measured homogeneous line shapes are Fourier limited [25–27]. The linewidth increases with pump power due to saturation broadening of the transition [blue symbols in Fig. 2(c)], which is consistent with the expected behavior for a
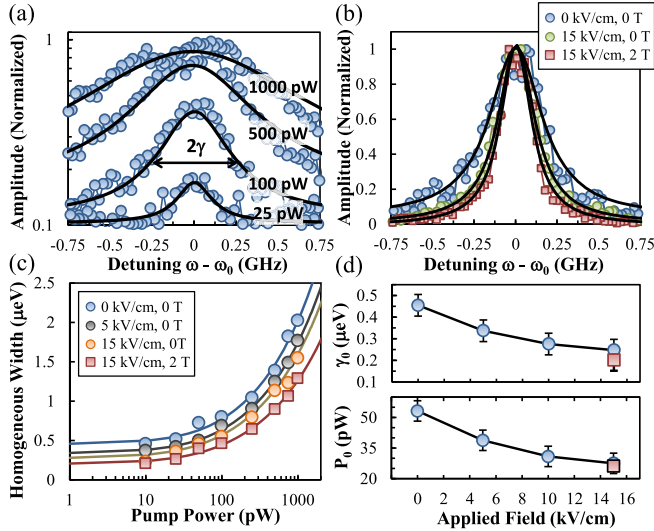
FIG. 2. (a) Homogeneous line shape as a function of pump laser power up to 1000 pW (points) and Lorentzian fit functions (solid lines). The half width at half maximum provides a measure of the homogeneous linewidth. (b) Homogeneous line shape for 100 pW pump power and an applied lateral field from 0–15 kV cm^{-1} (circles) and magnetic field in Faraday geometry (squares). The solid lines are Lorentzian fit functions. (c) Power broadening of the homogeneous linewidth (symbols) for applied field up to 15 kV cm^{-1}. A fit of Eq. (1) (solid lines) reveals that both the zero-power linewidth, γ_0, and saturation power, P_0, decrease with increasing field, shown in top and bottom panels in (d), respectively. The square data points are in the presence of a 2 T magnetic field in Faraday configuration.

resonantly driven, two-level system. Saturation broadening of the linewidth can be expressed as

$$\gamma = \frac{\gamma_0}{2}\sqrt{1 + P/P_0}, \qquad (1)$$

where P is the pump power, P_0 is the power required to saturate the absorption, and γ_0 is the transition linewidth in the absence of saturation effects [28]. The zero-power limit of the fit [solid blue line in Fig. 2(c)] is used to determine a linewidth of $\gamma_0 = 0.45 \pm 0.05$ μeV ($T_2 = 1.46 \pm 0.07$ ns), which is consistent with previously measured population-lifetime limited linewidths and indicates that additional pure dephasing mechanisms are absent [8,9]. From the same fit, we extract a saturation power $P_0 = 53 \pm 5$ pW. Since a precise determination of the pump power coupled to the QDs is difficult, this value only provides an estimate of this fundamental property of light-matter interaction. Nonetheless, relative changes of P_0 contain useful information on how easily the QD absorption saturates under different experimental conditions.

Our major results are illustrated by the homogeneous line shapes presented in Fig. 2(b) for 100 pW pump power. Upon applying a bias to the electrodes, the linewidth narrows, which occurs for all incident pump powers shown

in Fig. 2(c) for fields up to 15 kV cm^{-1}. The linewidth exhibits saturation broadening behavior at all applied field strengths, which is fit using Eq. (1) to determine how the field influences γ_0 and P_0. Both the linewidth and saturation power decrease monotonically to $\gamma_0 = 0.25 \pm 0.05$ μeV and $P_0 = 28 \pm 5$ pW at 15 kV cm^{-1} [Fig. 2(d)]. At larger fields, the linewidth increases suggesting the onset of charge carrier tunneling out of the QDs. Because the homogeneous line shapes are primarily governed by radiative recombination (see below), narrowing of the linewidth with increasing field also reflects a reduction in the radiative recombination rate and, thus, the oscillator strength, of the trion transition. Although radiative recombination dominates, our previous work has shown that precession of the trion-bound electron spin about the Overhauser magnetic field created by the ~10^5 nuclear spins in the QD results in additional slow decoherence [9]. This hyperfine-mediated broadening can be screened by a moderate magnetic field in the Faraday configuration, which is confirmed, here, by additional linewidth narrowing to $\gamma_0 = 0.20 \pm 0.05$ μeV ($T_2 = 3.29 \pm 0.07$ ns) for a magnetic field strength of 2 T [red squares in Fig. 2(d)]. Along with the ability to electrically control the coherence time, the linewidth of 0.20 μeV is the narrowest reported for group III–V QDs to date. We focus on changes in the line shape, here, because it is the least sensitive to systematic errors, but fits to the absolute change in absorption yield consistent results and are shown in the Supplemental Material [22].

These results demonstrate that the applied field decreases the trion transition dipole moment, consequently increasing the coherence time. To illustrate this, we express the linewidth and saturation power in terms of the radiative lifetime (T_1), coherence time (T_2), and transition dipole moment (μ) through the relations $\gamma_0 = 1/2(\Gamma + \Gamma')$ and $P_0 \propto (T_1 T_2 \mu^2)^{-1}$, where $\Gamma' = 0.05$ μeV equals the hyperfine interaction broadening [9,28]. Additionally, the radiative lifetime can be related to the transition dipole moment through $T_1 \propto \mu^{-2}$. After inserting these expressions into Eq. (1), we obtain

$$\gamma = \frac{1}{4}(\mu^2 + \Gamma')\sqrt{1 + \frac{P}{2(\mu^2 + \Gamma')}}, \qquad (2)$$

which is a simple expression relating the linewidth power broadening to relative changes in the transition dipole moment. We show, in Fig. 3(b) (points), the normalized transition dipole moment extracted from the linewidth fits as a function of electric field, normalized to the zero-field value. With increasing field up to 15 kV cm^{-1}, the dipole moment decreases by 30%. Interestingly, screening of the hyperfine interaction by an external magnetic field results in a narrower linewidth without affecting the transition dipole moment [square symbol in Fig. 3(b)]; i.e., the hyperfine-mediated broadening introduces additional decoherence to the system without reducing the radiative efficiency. This result is
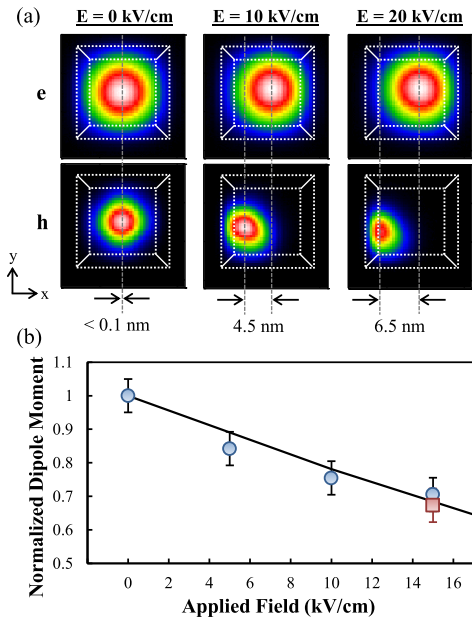
FIG. 3. (a) Single-band effective-mass calculations of the single-electron (top row) and two-hole (bottom row) wave functions as a function of applied lateral electric field. (b) Calculated (solid line) and measured (symbols) transition dipole moment as a function of applied electric field. The square data point is in the presence of a 2 T magnetic field in Faraday configuration.

consistent with our measurements of similar saturation powers with and without the Faraday magnetic field shown in Fig. 2(d).

We rule out a quantum-confined Stark shift [29–31] as a source of linewidth narrowing, which could shift QDs with a smaller linewidth into resonance with the pump, by measuring homogeneous line shapes for QD emission at 1045 nm (see Supplemental Material [22]). We obtain $\gamma = 0.50 \pm 0.05$ μeV at 0 kV cm^{-1} and 25 pW pump power, equal to the value obtained when tuned to 1050 nm (0.52 ± 0.05 μeV). Equivalent values are also measured for a 1 nW pump power (2.03 ± 0.05 μeV and 2.11 ± 0.05 μeV at 1050 nm and 1045 nm, respectively). Therefore, we attribute the decrease in the transition dipole moment, leading to a longer coherence time, to a large in-plane static dipole moment created by the electric field.

To support our assertion that the enhanced coherence time arises due to a reduction in the trion transition oscillator strength, we numerically model electric field effects on the electronic wave functions using a single-band effective-mass Hamiltonian including a full treatment of piezoelectric effects and strain [32,33]. We consider QDs with uniform composition profiles that are square-based truncated pyramids with a 20 nm base and 5 nm height (see Supplemental Material [22]). In Fig. 3(a), we show normalized in-plane single electron and two-hole wave function probabilities. For increasing field strength along the x direction up to

20 kVcm^{-1}, the electron and two-hole wave functions are displaced in opposite directions, with the holes shifted to lower values along the y direction due to the built-in piezoelectric charges. A field of 15 kV cm^{-1} leads to an in-plane dipole moment per unit charge of $\sim$6 nm. The electron-hole separation decreases the overlap integral of the wave functions resulting in a weaker transition dipole moment [solid line, Fig. 3(b)]. The model nicely reproduces the measured dipole moment extracted from the power broadening measurements (symbols), which provides additional evidence that the homogeneous line shapes are lifetime limited. The lateral dipole moment is nearly an order of magnitude larger than the permanent dipole moment measured in vertical field-effect devices [34], demonstrating the advantage of the lateral field geometry for wave function manipulation. Calculations were also performed to model electric field effects on the exciton dipole moment in neutral QDs (Supplemental Material [22]). Qualitatively similar trends are obtained.

Electronic control of the excitonic dipole moment and coherence time provides new opportunities for integrated QD photonics and quantum information processing. For example, quantum operations of electronic spin qubits can be performed with the trion transition acting as an intermediary state. The ability to tune the trion transition dipole moment provides an additional control knob for rotating the electronic spin about the Bloch sphere. The large transition dipole moment also makes QDs particularly attractive as efficient nonclassical light sources. Scaling beyond a single QD for quantum computing and communication requires that different QDs generate indistinguishable photons [35], which may benefit from the Fourier-limited coherence control demonstrated here. Moreover, the large field-induced, in-plane static dipole moment might facilitate scalable two-qubit quantum logic gates through the dipole-dipole interaction. Previous work has demonstrated weak dipolar coupling ($\sim$30 μeV) between neighboring QDs, the strength of which depends on the dipole moment squared [36]. The calculated increase in the lateral dipole moment by over an order of magnitude with applied field implies a more than 100-fold increase in the dipolar coupling strength—sufficient to implement nonlocal conditional quantum logic [37]. These effects could be enhanced by tailoring the QD morphology to optimize the confinement potential for maximal wave function separation. We anticipate the results presented here will motivate additional studies investigating novel solid-state coherent control and coupling schemes using semiconductor QDs.

[1] P. Borri, W. Langbein, S. Schneider, U. Woggon, R. L. Sellin, D. Ouyang, and D. Bimberg, Phys. Rev. Lett. **87**, 157401 (2001).

[2] D. Press, T. D. Ladd, B. Zhang, and Y. Yamamoto, Nature (London) **456**, 218 (2008).

[3] W. B. Gao, P. Fallahi, E. Togan, J. Miguel-Sanchez, and A. Imamoglu, Nature (London) **491**, 426 (2012).

[4] M. T. Rakher, N. G. Stoltz, L. A. Coldren, P. M. Petroff, and D. Bouwmeester, Phys. Rev. Lett. **102**, 097403 (2009).

[5] A. Kiraz, M. Atature, and A. Imamoglu, Phys. Rev. A **69**, 032305 (2004).

[6] E. B. Flagg, A. Muller, S. V. Polyakov, A. Ling, A. Migdall, and G. S. Solomon, Proc. SPIE, Advances in Photonics of Quantum Computing, Memory, and Communication IV **7948**, 794818 (2011).

[7] J. J. Berry, M. J. Stevens, R. P. Mirin, and K. L. Silverman, Appl. Phys. Lett. **88**, 061114 (2006).

[8] V. Cesari, W. Langbein, and P. Borri, Phys. Rev. B **82**, 195314 (2010).

[9] G. Moody, M. Feng, C. McDonald, R. P. Mirin, and K. L. Silverman, Phys. Rev. B **90**, 205306 (2014).

[10] C. Santori, D. Fattal, J. Vuckovic, G. Solomon, and Y. Yamamoto, New J. Phys. **6**, 89 (2004).

[11] D. Englund, D. Fattal, E. Waks, G. Solomon, B. Zhang, T. Nakaoka, T. Arakawa, Y. Yamamoto, and J. Vuckovic, Phys. Rev. Lett. **95**, 013904 (2005).

[12] J. P. Reithmaier, G. Sek, A. Loffler, C. Hofmann, S. Kuhn, S. Reitzenstein, L. V. Keldysh, V. D. Kulakovskii, T. L. Reinecke, and A. Forchel, Nature (London) **432**, 197 (2004).

[13] K. Hennessy, A. Badolato, M. Winger, D. Gerace, M. Atature, S. Gulde, S. Falt, E. L. Hu, and A. Imamoglu, Nature (London) **445**, 896 (2007).

[14] M. M. Vogel, S. M. Ulrich, R. Hafenbrak, P. Michler, L. Wang, A. Rastelli, and O. G. Schmidt, Appl. Phys. Lett. **91**, 051904 (2007).

[15] B. Alen, J. Bosch, D. Granados, J. Martinez-Pastor, J. M. Garcia, and L. Gonzalez, Phys. Rev. B **75**, 045319 (2007).

[16] A. F. Jarjour, R. A. Oliver, A. Tahraoui, M. J. Kappers, C. J. Humphreys, and R. A. Taylor, Phys. Rev. Lett. **99**, 197403 (2007).

[17] A. J. Bennett, R. B. Patel, J. Skiba-Szymanska, C. A. Nicoll, I. Farrer, D. A. Ritchie, and A. J. Shields, Appl. Phys. Lett. **97**, 031104 (2010).

[18] D. Reuter, V. Stavarache, A. D. Wieck, M. Schwab, R. Oulton, and M. Bayer, Physica (Amsterdam) **32E**, 73 (2006).

[19] B. Krummheuer, V. M. Axt, and T. Kuhn, Phys. Rev. B **65**, 195313 (2002).

[20] J. W. Robinson, J. H. Rice, K. H. Lee, J. H. Na, R. A. Taylor, D. G. Hasko, R. A. Oliver, M. J. Kappers, C. J. Humphreys, and G. A. D. Briggs, Appl. Phys. Lett. **86**, 213103 (2005).

[21] B. D. Gerardot, S. Seidl, P. A. Dalgarno, R. J. Warburton, D. Granados, J. M. Garcia, K. Kowalik, O. Krebs, K. Karrai, A. Badolato, and P. M. Petroff, Appl. Phys. Lett. **90**, 041101 (2007).

[22] See Supplemental Material at http://link.aps.org/supplemental/10.1103/PhysRevLett.116.037402 for details of the device fabrication and experimental setup.

[23] H. Kamada and T. Kutsuwa, Phys. Rev. B **78**, 155324 (2008).

[24] M. Sargent, Phys. Rep. **43**, 223 (1978).

[25] H. Haug and S. W. Koch, Quantum Theory of the Optical and Electronic Properties of Semiconductors (World Scientific, Singapore, 1993).

[26] N. H. Bonadeo, G. Chen, D. Gammon, and D. G. Steel, Phys. Status Solidi B **221**, 5 (2000).

[27] J. Cheng, W. Yao, X. Xu, D. G. Steel, A. S. Bracker, D. Gammon, and L. J. Sham, Phys. Rev. B **77**, 115315 (2008).

[28] L. Allen and J. H. Eberly, Optical Resonance and Two-Level Atoms (Dover Publications, New York, 1987).

[29] H. Gotoh and H. Ando, J. Appl. Phys. **82**, 1667 (1997).

[30] H. Gotoh, H. Kamada, H. Ando, and J. Temmyo, Appl. Phys. Lett. **76**, 867 (2000).

[31] J. Seufert, M. Obert, M. Scheibner, N. A. Gippius, G. Bacher, A. Forchel, T. Passow, K. Leonardi, and D. Hommel, Appl. Phys. Lett. **79**, 1033 (2001).

[32] Using NEXTNANO software available at www.nextnano.com.

[33] C. Pryor, Phys. Rev. B **57**, 7190 (1998).

[34] J. J. Finley, M. Sabathil, P. Vogl, G. Abstreiter, R. Oulton, A. I. Tartakovskii, D. J. Mowbray, M. S. Skolnick, S. L. Liew, A. G. Cullis, and M. Hopkinson, Phys. Rev. B **70**, 201308 (2004).

[35] A. J. Bennett, R. B. Patel, C. A. Nicoll, D. A. Ritchie, and A. J. Shields, Nat. Phys. **5**, 715 (2009).

[36] T. Unold, K. Mueller, C. Lienau, T. Elsaesser, and A. D. Wieck, Phys. Rev. Lett. **94**, 137404 (2005).

[37] E. Biolatti, R. C. Iotti, P. Zanardi, and F. Rossi, Phys. Rev. Lett. **85**, 5647 (2000).